ELSEVIER

Nuclear Instruments and Methods in Physics Research A 438 (1999) 265–276

NUCLEAR INSTRUMENTS & METHODS IN PHYSICS RESEARCH Section A

www.elsevier.nl/locate/nima

Electron beam characteristics of a laser-driven plasma wakefield accelerator

K.A. Assamagan[a,*], W.W. Buck[a,b], S.-Y. Chen[c], R. Ent[b], R.N. Green[a], P. Gueye[a], C. Keppel[a,b], G. Mourou[c], D. Umstadter[c], R. Wagner[c]

[a]*Nuclear/High Energy Physics Research Center, Department of Physics, Hampton University, Hampton, VA 23668, USA*
[b]*Thomas Jefferson National Accelerator Facility, Newport News, VA 23606, USA*
[c]*Center for Ultrafast Optical Science, University of Michigan, Ann Arbor, MI 48109, USA*

Received 7 January 1999; received in revised form 9 July 1999; accepted 9 July 1999

Abstract

The properties of an electron beam trapped and accelerated in a laser wakefield have been investigated. Plastic scintillating fibers were employed together with position sensitive photomultiplier tubes (PMT) and a series of dipole electro-magnets to study the beam. The measured momentum spectrum peaks around 7 MeV/c with an exponential fall-off at high momenta up to (70.3 ± 19.9) MeV/c. The number of electrons detected per bunch is determined to be $(2.6 \pm 0.3) \times 10^{11}$.

PACS: 29.27.Fh; 29.40.Mc; 52.75.Di

1. Introduction

Recent developments in the high-peak-power lasers may revolutionize the technology for electron acceleration [1]. At the Center for Ultrafast Optical Science (CUOS) in University of Michigan, a technique termed "chirped pulse amplification" has been employed to produce a table-sized laser with a pulse duration of 400 fs and a maximum energy of 2 J [2]. The peak power of this laser reaches 5 TW, producing electromagnetic intensities exceeding 3×10^{18} W/cm^2. This laser beam impinges on a helium gas jet, creating a plasma by tunneling ionization and exciting an electron plasma wave through Raman forward scattering instability. The electric field in such an electron wave can accelerate electrons to a few GeV in one centimeter in principle [3].

The development of table-top electron accelerator is interesting to the electron scattering community since at large accelerator laboratories, total particle acceleration distances are measured in kilometers. At the CUOS facility, upwards of 10^{11} electrons are produced within a time window of 400 fs with a large photon background from interactions in the vacuum chamber wall, the collimators and the beam pipe. Conventional nuclear physics detection techniques are not well suited for the

* Corresponding author. Correspondence address: CERN, EP Division, CH-1211 Geneva 23, Switzerland. Tel.: + 41-22-767-1171; fax: + 41-22-767-8350.

E-mail address: ketevi.assamagan@cern.ch (K.A. Assamagan)

0168-9002/99/$ - see front matter
PII: S0168-9002(99)00882-7

study of such a beam. Therefore, the challenge was to develop a specific diagnostic method to measure the beam characteristics (beam energy, profile, intensity, etc). Such a method is presented in this paper along with the results obtained.

2. Description of the apparatus

The interaction between the laser pulse and the gas jet occurs in a vacuum chamber evacuated to $\sim 10^{-1}$ Torr. A fraction of the electrons produced exit the chamber through an aperture of 2.54 cm long and 7.63 cm diameter. The chamber is spherical with a radius of 59.7 cm. The detector was aligned in the beam line behind the exit flange. To shield against background radiation from particles hitting the vacuum chamber walls and exiting anywhere else other than through the flange, a lead wall of $119.4 \times 119.4 \times 10.2\,\mathrm{cm}^3$ was erected around the flange, isolating the detector from the chamber as shown in Fig. 1.

The detector consisted of two arrays of plastic scintillating fibers enclosed in a lightproof box. Each array comprised sixteen fibers of $3\,\mathrm{mm} \times 3\,\mathrm{mm} \times 150\,\mathrm{mm}$ and was coupled to a position-sensitive photomultiplier tube (Hamamatsu H6568) which has 16 independent input and output channels. During the measurements of the spatial profile of the beam, the two scintillator arrays were joined to form a single array of 32 fibers which was then placed behind the lead shielding to cover the entire area of the flange (item 5 of Fig. 1). The 32 output signals were sent to Analog-to-Digital Converters (ADC, LeCroy 2249A) which were gated by a signal synchronized with the laser pulse. The readout and the on-line analysis were carried out with a data acquisition system designed specifically for this project [4].

The rest of the detector consisted of a collimator (1 cm in diameter, $\sim$ 10 cm long), and three dipole electro-magnets, each having 12.6 cm effective length, 2.7 cm gap and a field integral of 4200 Gauss-cm at a current of 4 A. During the measurements of the momentum distribution, one of the scintillating fiber arrays was positioned behind a lead collimator at 6° from the axis of the electron beam propagation defined by the first collimator. The other fiber array detector was placed at zero degree, also behind a lead collimator as shown in Fig. 1 (items 13). Both detectors were at 130 cm from the flange. The momentum distribution of the electrons was measured with the detector at 6° by varying the current in the magnets, while undeflec-

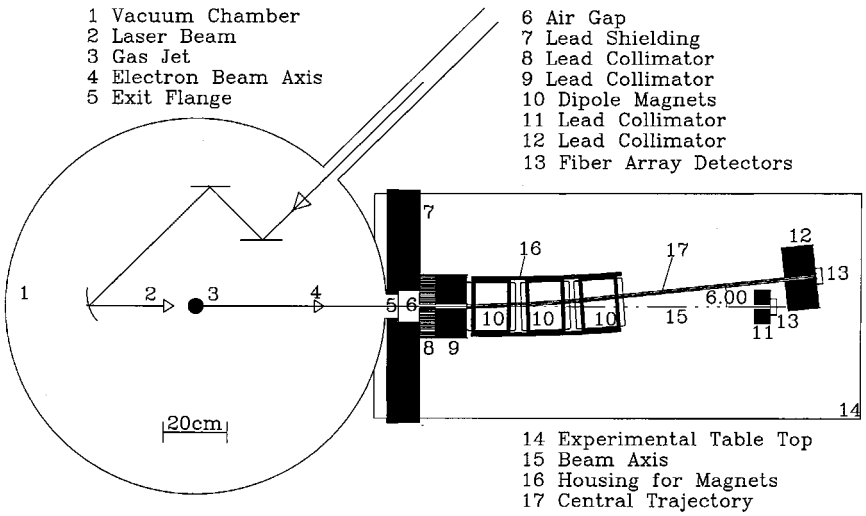

Fig. 1. A sketch of the experimental setup for the current scan. The beam pipe, not shown here, extended the vacuum from the flange to the detectors. The pipe was made of two stainless steel tubes welded at an angle of 6°. The detector at 6° did not see the source (item 3).

ted particles were detected by the fiber array at zero degree. A stainless-steel beam pipe was attached to the flange via a bellow which facilitated alignment. The pipe was made of two tubes welded together at an angle of 6°. When attached to the flange, the beam pipe extended the vacuum along the 0° and the 6° lines up to the entrance of the detectors (items 13 of Fig. 1).

The laser was operated at a rate of once every 3 or 10 min depending on the laser energy. The low repetition rate is necessary to cool the laser. The time structure of the electron beam is similar to that of the laser beam, i.e., the electron pulse duration is $\sim$400 fs at the same repetition rate as the laser pulse. In prior measurements [5], the electron beam emittance was found to be $\sim 0.5\pi$ mm·mrad ($10^\circ \times 8.5\,\mu$m). The entire electron beam distribution impinged on the detector within 400 fs resulting in large energy depositions depending on the number of electrons produced – a minimum ionizing electron deposits $\sim$ 600 keV in a 3 mm-thick plastic scintillator [6]. For this reason, the fiber light output was kept at the level which ensured the operation of the PMTs in their linear regime: the fibers were polished only at one end and they were grease-coupled to the PMTs. They were still wrapped in aluminized mylar to eliminate cross-talk. To measure the beam characteristics, we calibrated the detector with minimum ionizing electrons from a radioactive source. The ratio of the detector response to the beam and to the source is then the equivalent number of minimum ionizing electrons in the beam.

The background in this experiment was made of secondary particles (electrons, positrons and medium energy photons) from electromagnetic showers or scattering in the collimators, the beam pipe and the lead shielding. The structure of the primary electron beam (very short pulse duration and large emittance) rendered the suppression of the background extremely difficult.

3. Detector calibration

Data were taken at different settings of applied voltage on the PMTs and at different current settings in the electro-magnets. For accurate normalization, it was necessary to operate the detectors in their linear regime, and to understand the detector efficiencies as a function of applied voltage. The plastic fibers (F) were sandwiched between two plastic scintillator detectors (S1 and S2). Particles from a ^{228}Th source placed on S1, traversed all the three detectors. The efficiencies were measured as the ratio of the rates $S1 \cdot F \cdot S2$ and $S1 \cdot S2$. The results are shown in Fig. 2. The detector efficiencies become uniform and converge to about 50% at voltages between 650 and 900 V. However, the detectors were operated between 400 and 800 V because large fluctuations in the number of electrons sometimes saturated the ADCs, especially at higher applied voltages.

It was necessary to verify the linearity of the system in order to normalize the data taken at different voltages. The linearity was measured as the response of the fiber detectors to minimum ionizing electrons from the source at different applied voltages. As shown in Fig. 3, both detectors are linear between 500 and 800 V where most of the data were taken. Below 500 V, the responses were too small to be measured with good precision even after amplifications. Therefore, we extrapolated these linearity curves for the data taken at 400 V.

The field as a function of current was measured at the center of each magnet and the results are shown in Fig. 4. The central momentum P_0 corresponding to the current setting was estimated from

$$P_0(\mathrm{MeV}/c) = \frac{0.3 \times 10^{-3}}{\theta_0(\mathrm{rad})} \int B\,\mathrm{d}l(\mathrm{kG\ cm}) \tag{1}$$

assuming a uniform field in the region of the particle trajectory that was consistent with a deflection of $\theta_0 = 6^\circ$. The equivalent number N of minimum ionizing electrons observed in the detector is given as

$$N = \frac{(S - B)}{Q_0 \times \varepsilon} \tag{2}$$

where $(S - B)$ is the background subtracted detector signal, ε is the efficiency of the detector and Q_0 is the detector response to minimum ionizing electrons from the ^{228}Th source.

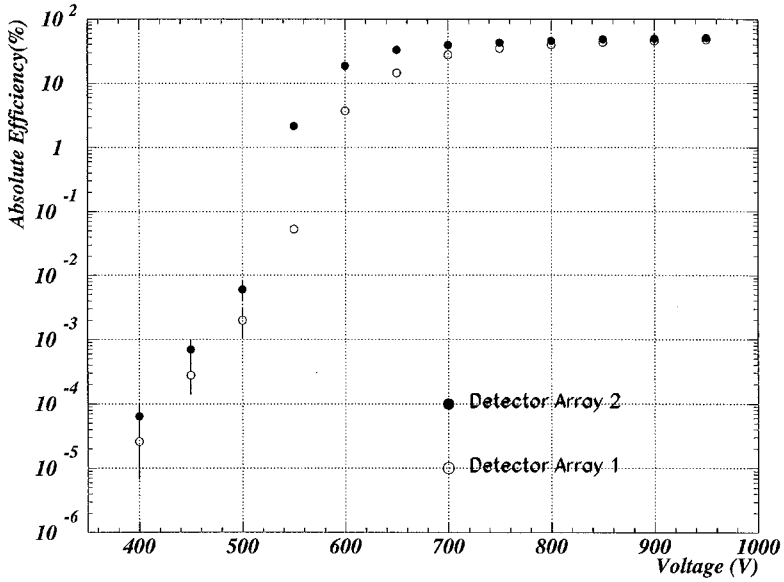

Fig. 2. Efficiencies of the arrays of plastic scintillating fibers used as a function of applied voltage. Each detector consisted of 16 fibers viewed by a position sensitive PMT with 16 independent input and output channels.

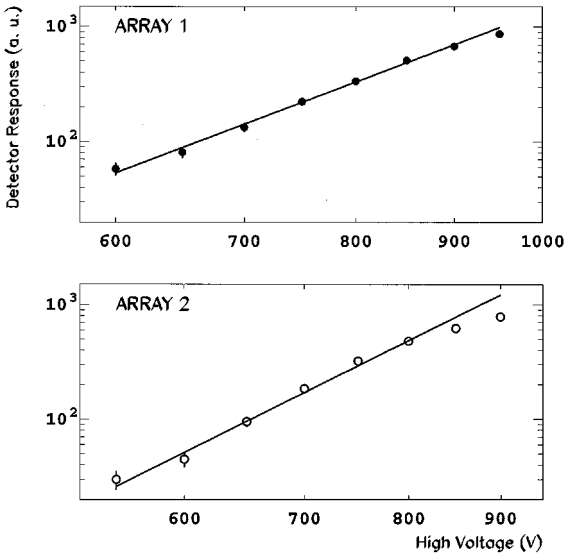

Fig. 3. The linearities of the detectors as a function of voltage. The detectors were operated between 400 and 800 V during these measurements. The data are shown on a log–log scale.

4. Spatial distribution

We measured the spatial profile of the electron beam at the flange by connecting both detectors side by side to form a single array of 32 plastic scintillating fibers. The detector was placed just behind the lead shielding (item 7 of Fig. 1, 69.7 cm away from the electron source). This arrangement allowed only the measurement of the horizontal profile of the beam. When the entire face of the exit flange was shielded, we observed no response from the detector above discrimination level set slightly higher than the detector noise level (the average count in the ADCs was 50 channels, i.e., the level of the ADC pedestals). This demonstrated the effectiveness of the lead shielding in eliminating particles which exited the vacuum chamber at places other than through the flange. The response of the detector at the flange is fitted to a function of the form

$$g(x) = a\cos^2(b(x-c)) + d \tag{3}$$

which should describe the profile of the flange as seen by the detector assuming a uniform background (the parameter d of Eq. (3)). The result is shown in Fig. 5. The diameter of the flange was 76.2 mm while the detector covered an effective distance of 96 mm. Therefore, the plastic fibers at the positions $|x| > 38.05$ mm should not have fired. The spectrum of Fig. 5 suggests that the exit flange was

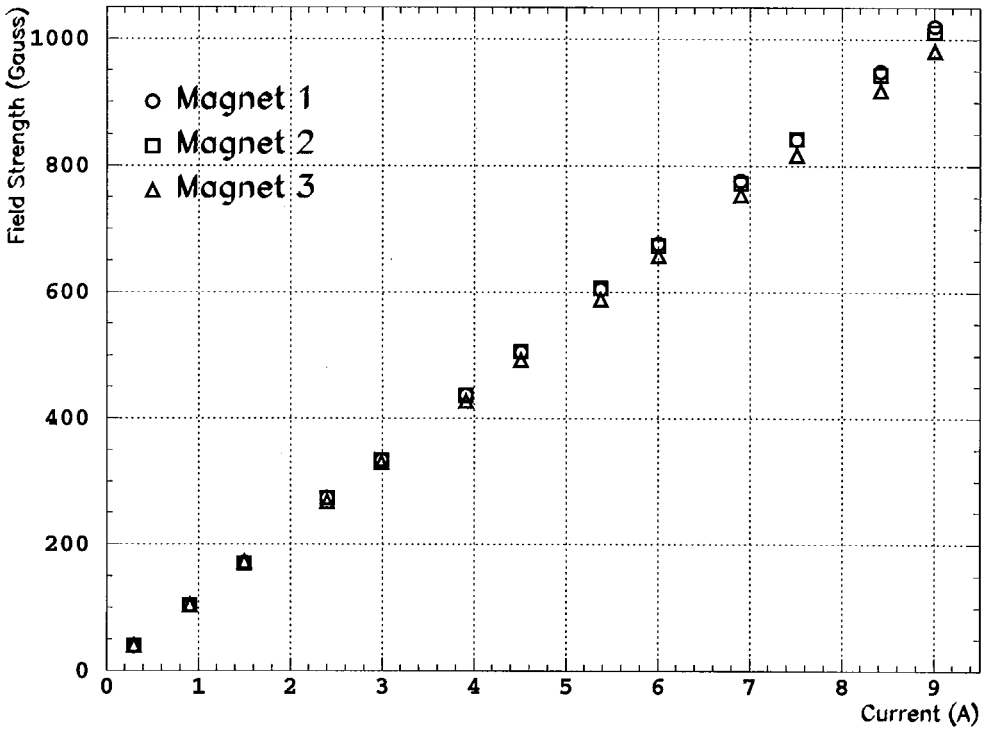

Fig. 4. The field strength at the center of the magnet as a function of current for each of the three dipole magnets used.

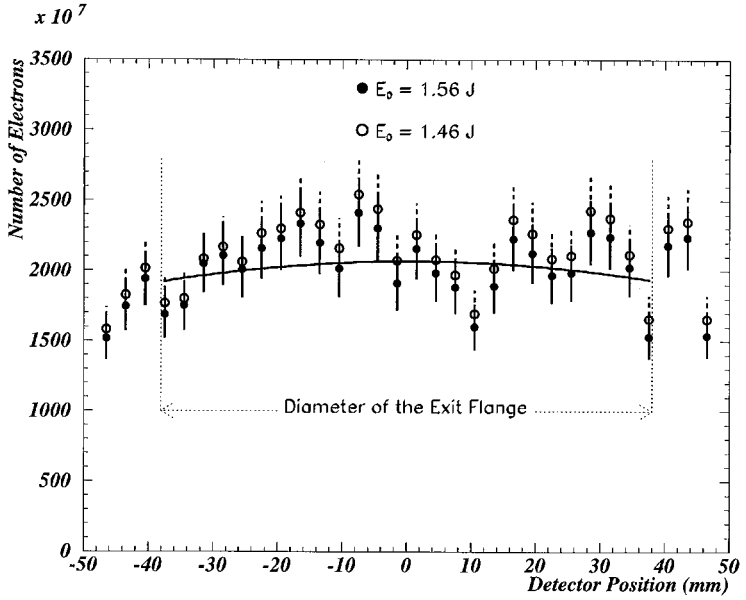

Fig. 5. The measured horizontal spatial distribution at the exit of the interaction chamber. For this measurement, the detectors were arranged to form a single array of 32 plastic fibers placed behind the lead shield (Fig. 1). The solid line is a $\cos^2$ fit to the data showing the expected profile assuming a uniform background. Data taken at two different settings of the laser energy E_0 show essentially the same distribution.

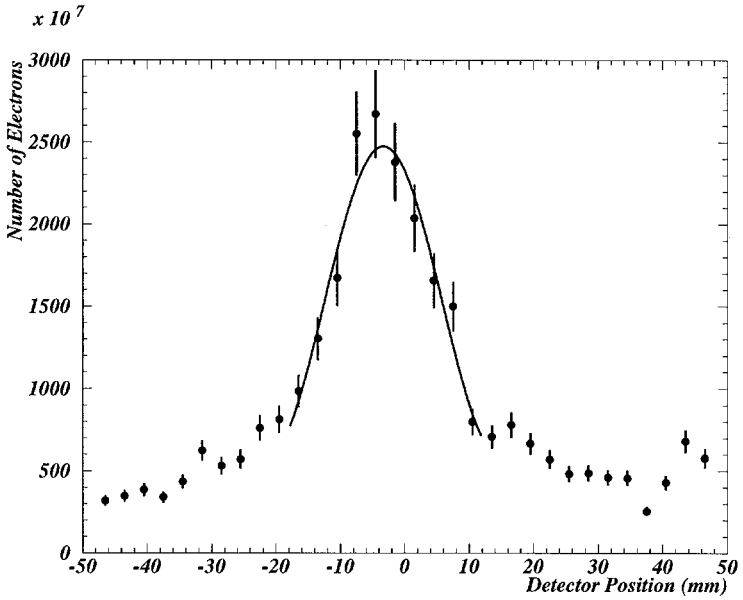

Fig. 6. The profile of the 1-cm diameter collimator as seen by the single array of 32 plastic fibers. In this measurement, the detector was installed behind the collimator (items 8 and 9 of Fig. 1). The solid curve is a $\cos^2$ fit of the form given by Eq. (3). The peak is off-centered because of detector misalignment.

not a good collimator: secondary particles from showers and scattering were not suppressed effectively and contributed significantly to the response of the plastic fibers positioned at $|x| > 38.05$ mm. Indeed, we placed the entire 32 plastic fibers as a single detector just behind the 1-cm diameter collimator (items 8 and 9 of Fig. 1, 10 cm long). The response of the detector showed the profile of the collimator as seen in Fig. 6. Here, much of the background was eliminated but, the plastic fibers outside the effective area of the collimator still detected some scattered or shower particles inside the collimator – the average count in the ADCs of the outside plastic fibers ($|x| > 38.05$ mm) was 100 channels as opposed to 50 (ADC pedestal) for the null experiment when the face of the exit flange was entirely shielded. One would extract the profile of the beam from the data of Fig. 5 by a deconvolution of the collimator effects given by Eq. (3) which assumes a uniform background. Such a procedure leads to a beam profile which is not significantly different from Fig. 5 and could be interpreted as being uniform.

5. Energy spectrum with degraders

The energy distribution was first measured with passive aluminum degraders of various thicknesses inserted in the electron beam just upstream of the detector positioned against the lead wall (item 7 of Fig. 1). The degraders were inserted in the air gap (item 6). Each degrader thickness X_i (cm) corresponds to a threshold energy E_i which is the minimum energy that an electron must possess to traverse the degrader and arrive at the detector. As the thickness of the degrader was increased, fewer electrons arrived at the detector and the charges (as measured in the ADCs) decreased accordingly. Table 1 shows the degrader thickness X_i, the corresponding threshold energy E_i (MeV), and the number of electrons observed above the energy E_i. The values of E_i were obtained from the range of electrons in aluminum [5]. The critical energy of aluminum is 51 MeV. Therefore, for the thicknesses shown in Table 1, the dominant process of energy loss is ionization, except for $X_i = 7.62$ and 10.16 cm. For each degrader inserted in the beam, the

Table 1
The absorber thicknesses X_i (cm), the threshold energies E_i (MeV), the normalized number of electrons $N_i(E > E_i)$ with energy $E > E_i$, the mean energies $\bar{E}_i$ and the normalized number of electrons per MeV $n_i(\bar{E}_i)$

X_i (cm)	E_i (MeV)	$N_i(E > E_i)$	$\bar{E}_i$ (MeV)	$n_i(\bar{E}_i)$
0.000	0.00	7.23×10^9		
			0.23	7.58×10^9
0.079	0.45	5.91×10^9		
			0.68	10.16×10^9
0.159	0.90	4.28×10^9		
			1.16	1.97×10^9
0.238	1.41	3.18×10^9		
			1.62	1.14×10^9
0.318	1.82	2.68×10^9		
			2.02	0.91×10^9
0.397	2.22	1.09×10^9		
			2.43	0.53×10^9
0.476	2.63	0.86×10^9		
			2.83	0.35×10^9
0.556	3.03	7.03×10^9		
			3.23	0.17×10^9
0.635	3.43	0.63×10^9		
			5.01	0.07×10^9
1.270	6.70	0.52×10^9		
			9.90	0.09×10^8
2.540	13.10	0.46×10^9		
			16.35	0.15×10^8
3.810	19.60	3.54×10^9		
			25.30	0.04×10^8
5.080	31.00	2.94×10^9		
			40.30	0.03×10^8
7.620	49.50	2.47×10^9		
			59.80	0.01×10^8
10.160	70.00	2.20×10^9		

number of electrons $N_i(E > E_i)$ was extracted according to Eq. (2) but without background subtraction. From the $N_i(E > E_i)$s, the differential numbers of electrons were obtained

$$n_i(\bar{E}_i) = \frac{N_i(E > E_i) - N_i(E > E_{i+1})}{E_{i+1} - E_i} \tag{4}$$

with

$$\bar{E}_i = \frac{E_i + E_{i+1}}{2} \tag{5}$$

and

$$\Delta E_i = \frac{E_{i+1} - E_i}{2}. \tag{6}$$

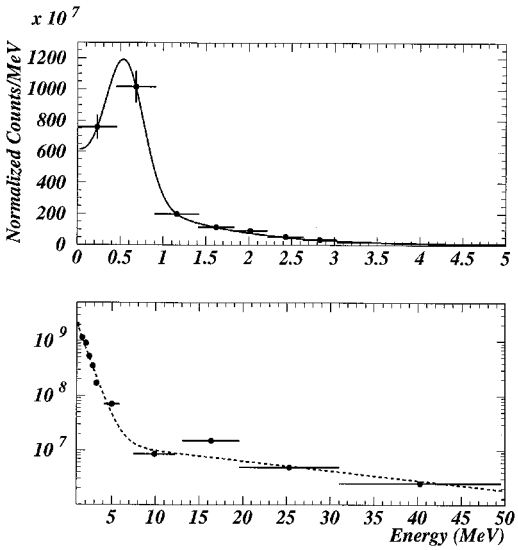

Fig. 7. The differential energy distribution measured with the aluminum degraders. Above ~ 0.5 MeV, the spectrum follows two exponentials with different slopes. The bottom panel is the same the top one but on a semi-log scale. The data taken with the degrader gave an idea on the beam characteristics and this was necessary for the design of the arrangement of Fig. 1, in particular the dipole magnets.

The energy distribution was obtained by plotting $n(\bar{E}_i)$ as a function of $\bar{E}_i$ as shown in Fig. 7. The data can be represented by the sum of two exponential functions and the distribution comprises mostly low energy electrons. The rate shown Fig. 7 is not necessarily the same as that of Fig. 5: the two data sets were taken with the detector positioned against the lead wall but at different times. Some parameters of the wakefiled acceleration (gas jet or laser properties) may have changed resulting in the change in the electron production rate.

The major difficulty with the absorber method is the production of secondary particles by electron bremsstrahlung in the aluminum. From the measurement of the spatial profile of the beam as shown in Fig. 5, the detector, positioned against the lead wall, already saw considerable amount of background from scattering in the flange. Furthermore, the insertion of degrader also changes the original distribution because of multiple scatterings and energy losses. Therefore, it was necessary

to study the beam characteristics with minimal interference with the original beam. The data from the degrader method did yield some understanding of the energy distribution and the highest electron energy in the beam, and this was necessary for the design of the apparatus of Fig. 1, in particular the dipole magnets.

6. Momentum distribution

We used the set-up of Fig. 1 to measure the number of electrons in the detectors placed at 0° and 6° (items 13) with respect to the nominal beam axis as a function of the current in the dipole magnets. Each detector had 16 plastic fibers, i.e., a coverage of 4.8 cm while the inside diameter of the beam pipe was 1 cm.

Two null tests were performed before the current scan itself: first, the flange was completely shielded out and we observed no response from the detector above the ADC pedestals. Secondly, with the arrangement of Fig. 1, we set the current in the dipole magnets to zero. This measurement set scale of the background in the detector at 6° whose response was of interest during the current scan. This background was due to re-scattered or electromagnetic shower particles (medium energy photons) which are difficult to stop.

For each setting, we recorded the set current and the field strength at the center of each magnet. The detector at 6° measured the number of particles with momentum P_0 given by Eq. (1). The undeflected particles were counted in the detector at 0° and served as a cross-check for our measurements. At a current setting of 0 A, all the particles were

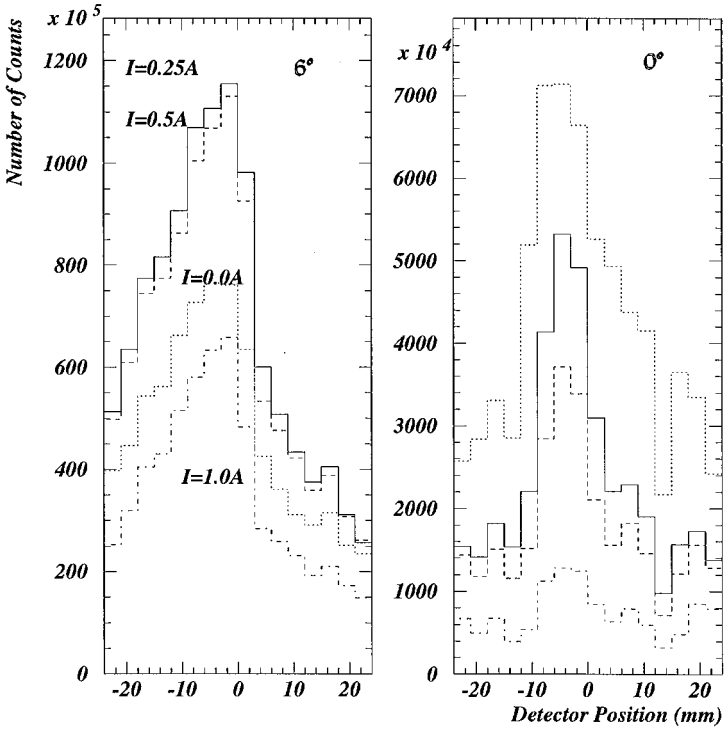

Fig. 8. The momentum scan showing the response of the detectors as a function of the current setting in the dipole magnets. Here, the current settings varied between zero and one ampère. The solid, dashed, dotted and dash–dotted lines correspond to 0.25, 0.5, 0 and 1 A current settings, respectively. At 1 A and above, we registered pulse heights smaller than the detector response at 0 A. This is because the momentum distribution is dominated by low energy electrons which are swept away at higher (>1 A) current settings.

expected in the 0° detector. However, because of scatterings in the collimators and in the beam pipe, a signal was seen in the 6° detector. As the current setting was increased, the pulse height in the 0° detector decreased with respect to the 0 A setting as expected while an increase in the response of the other detector was observed up to a current setting of 0.5 A. At 1 A and above, we registered in the detector at 6° pulse heights smaller than the detector response at 0 A as shown in Figs. 8 and 9. The peaks (corresponding to different current settings) in these figures are stable. This suggests that the data in Figs. 8 and 9 are a real momentum distribution instead of re-scatterings. Above the current setting of 4.5 A, the signals in both detectors disappeared and a uniform response was observed. These observations suggest that the momentum distribution comprises mostly low-energy electrons (≤ 0.5 A). At current setting above 1 A, the low-energy electrons are swept away resulting in smaller pulse heights in the detector at 6° as observed.

The signals in these figures are riding on substantial backgrounds coming from re-scatterings and electromagnetic showers. The subtraction of this background was performed by fitting the detector response with a function that is a linear combination of a Gaussian (the signal) and a polynomial (the background) as shown in Fig. 10. In most cases (Figs. 8 and 9 for instance), the assumption of a uniform background did not result in good fits. The momentum distribution is shown in Fig. 11. The distribution peaks around 7 MeV/c ($\cong 0.5$ A) with an exponential fall-off at higher momenta.

We replaced the stainless-steel pipe with a PVC pipe to reduce the scattering efficiency but the main results remained unchanged. This indicates that the scattering at 6° was not a major problem.

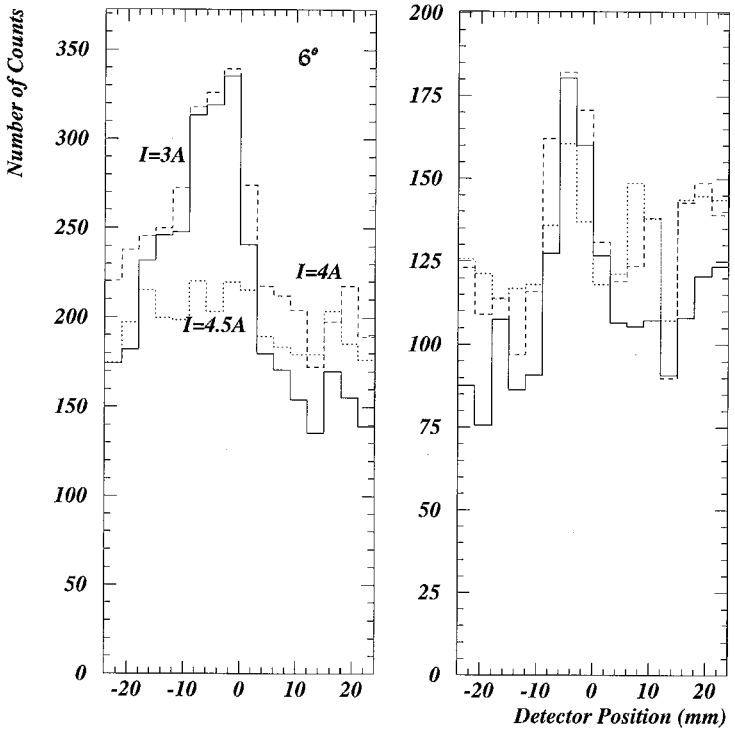

Fig. 9. The momentum scan showing the response of the detectors as a function of the current setting in the dipole magnets. Here, the current settings varied between 3 and 4.5 A. The solid, dashed and dotted lines correspond to 3.0, 4.0 and 4.5 A settings, respectively. At 4.5 A and above, the signal disappears and one sees only a uniform background. The right panel corresponds to the detector at 0°.

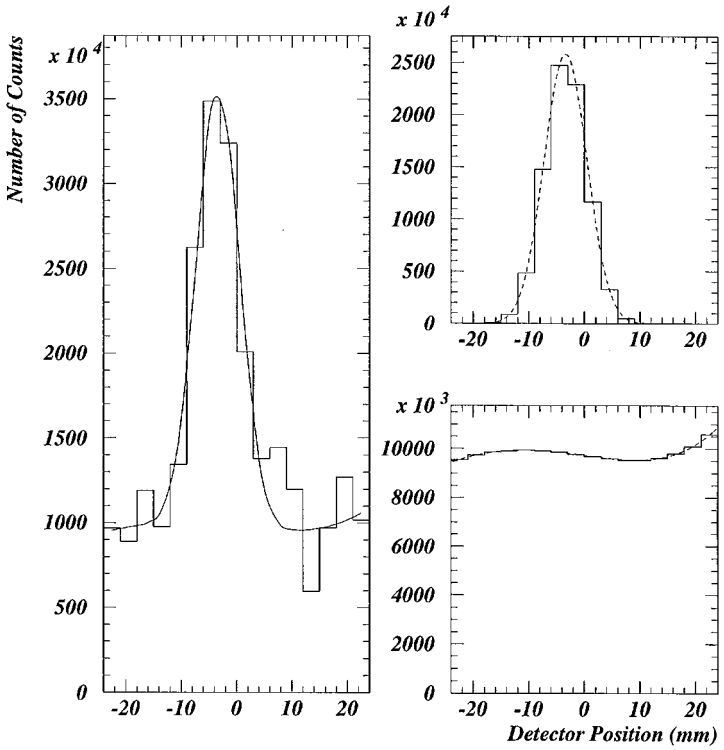

Fig. 10. Background subtraction. The data were fitted to a linear combination of a Gaussian and a polynomial functions. The signal was taken as the area under the Gaussian. The left panel shows the data with the fitting function. The top right is the signal. The background is shown in the bottom right panel.

7. High-momentum endpoint

The highest momentum in the beam was estimated from the fit to the data of Fig. 11 to be $P_{\max} = (32.5 \pm 6.7)$ MeV/c. The actual endpoint is higher; $P_{\max}$ is simply the value at which the background became so large that it was difficult to observe any statistically meaningful signal in the detector at 6°. At the current setting corresponding to 40 MeV/c, we observed some 219 events in the detector at 0°. These events are higher-energy electrons with some photon contamination. Assuming that all these events are electrons and that the distribution beyond 29 MeV/c is also exponential such that

$$\int_{29}^{\infty} C_0 \exp(C_1(P-29))\,\mathrm{d}P = 219 \pm \sqrt{219} \qquad (7)$$

we estimated the endpoint momentum to be $P_{\max} = (70.3 \pm 19.9)$ MeV/c.

8. Number of electrons in the beam

The average total number of electrons in a beam bunch can be estimated by integrating the spectrum of Fig. 11:

$$N_0 = \int_0^{\infty} f(P)\,\mathrm{d}P = (5.5 \pm 0.6) \times 10^8. \qquad (8)$$

However, N_0 is the number of electrons per bunch at the second collimator (item 12 of Fig. 1). The number of electrons N_T at the flange (item 5 of Fig. 1) scales as the ratio of the solid angle Ω_f of the flange, (7.62 cm diameter, 69.7 cm away from the source) to the solid angle Ω_c of the collimator (1 cm diameter, 199.7 cm from the source), i.e.,

$$N_T = \frac{\Omega_f}{\Omega_c} N_0 = (2.6 \pm 0.3) \times 10^{11}. \qquad (9)$$

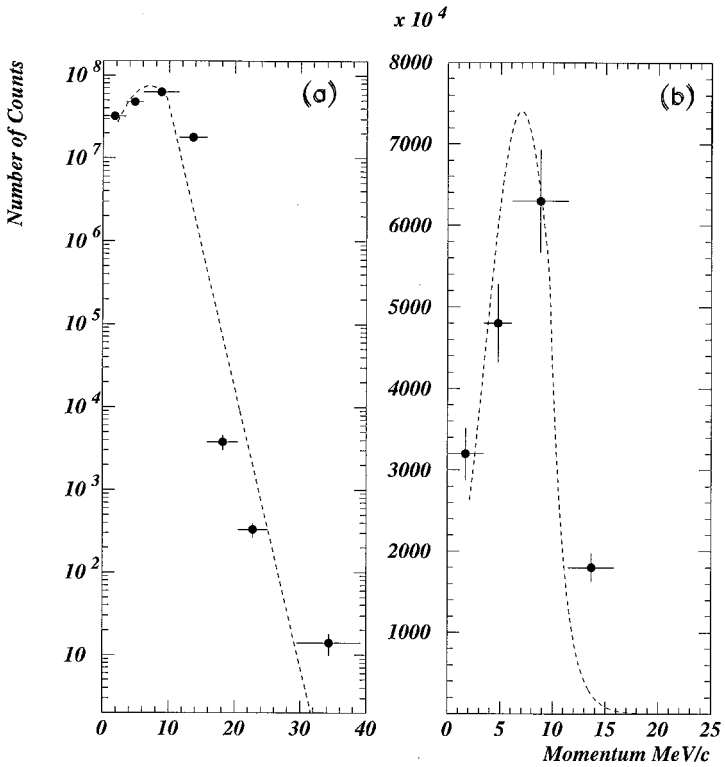

Fig. 11. The measured momentum distribution peaks around 7 MeV/c and falls exponentially at higher momenta. (a) The data are plotted on a semi-log scale. The dashed line is the fit. (b) The data are shown on a linear scale.

One can also estimate the number of electrons at the flange N_T by integrating directly the distribution of Fig. 5:

$$N_T = \int_{\Omega_f} g(x)\,dx = (5.3 \pm 0.6) \times 10^{11}. \quad (10)$$

The discrepancy between these two methods (Eqs. (9) and (10)) is due to the fact that the background was not subtracted from the spatial distribution $g(x)$ shown in Fig. 5.

9. Conclusions

We conducted a series of measurements with the aim to characterize the electron beam produced in the interaction of a high-power laser with a gas jet. We developed an acquisition system suited to the structure of the beam – the beam pulses were 400 fs long with a repetition rate of 3–10 min, with a large photon background. The detector consisted of plastic scintillating fibers viewed by position sensitive PMTs, dipole magnets, collimators and the readout electronics. The insertion of passive aluminum degraders in the beam revealed that the energy distribution consists of low-energy electrons and that the distributions can be represented as the sum of two exponential functions of different slopes. We also performed a current scan from which we extracted more accurately the momentum distribution and the highest electron energy in the beam. By calibrating the response of the scintillators with minimum ionizing electrons from a radioactive source, we estimated the equivalent number of minimum ionizing electrons per beam bunch to be of the order 10^{11}. However, this number is obtained outside the interaction chamber ($\sim$60 cm away from the interaction point, $\sim$8 cm-diameter). Therefore, the actual number of electrons produced

may be higher. The momentum spectrum shows a peak around 7 MeV/c with a higher energy exponential tail up to $\sim$70 MeV/c. We also measured the response of the detector at the exit of the interaction chamber. The spatial profile of the beam can be extracted from this measurement by deconvolving the effects of the exit flange which collimated the beam. This procedure leads to a distribution not much different from the measurement itself and can be interpreted as being uniform. A better knowledge of the spatial distribution requires a suppression or a better understanding of the background (Monte Carlo studies). Several improvements are being investigated currently for a precision measurement of the beam characteristics. Furthermore, improvements are underway in the wakefield production and acceleration system for the delivery of mono-energetic electrons at higher energy than has been observed thus far and at a higher duty cycle.

Acknowledgements

We wish to thank Dr. Charles Sinclair for discussions and for technical assistance and guidance. This work is supported by a grant from the National Science Foundation.

References

[1] E. Esarey, P. Sprangle, J. Krall, A. Ting, IEEE Trans. Plasma Sci. PS-24 (1996) 252.
[2] D. Umstadter, S.-Y. Chen, A. Maksimchuk, G. Mourou, R. Wagner, Science 273 (1996) 472.
[3] D. Umstadter, Laser Focus World 101–107 (1996).
[4] K.A. Assamagan, NuHEP Data Acquisition System, Hampton University, unpublished.
[5] R. Wagner, S.-Y. Chen, A. Maksimchuk, D. Umstadter, Phys. Rev. Lett. 78 (1997) 3125.
[6] W.R. Leo, Techniques for Nuclear and Particle Physics Experiments, Springer, Berlin, 1987.